# Reconfigurable All-Optical Code Translation in Spectrally Phase-Coded O-CDMA

Z. Jiang, *Student Member, IEEE*, D. S. Seo, *Member, IEEE*, D. E. Leaird, *Member, IEEE*, R. V. Roussev, C. Langrock, *Student Member, IEEE*, M. M. Fejer, *Fellow, OSA*, and A. M. Weiner, *Fellow, IEEE, Fellow, OSA*

***Abstract*—Reconfigurable all-optical code translation are demonstrated in a spectrally phase-coded optical-code-division multiple-access (O-CDMA) testbed with an interference user. For both one-stage and two-stage code translations, less than 0.9-dB power penalties are induced at each code translation. Multistage code translations are investigated via simulation and experimental emulation in a loop pulse shaper to show the potential application of the proposed method for up to several tens of code translations.**

***Index Terms*—Code translation, multiple-access interference, optical-code-division multiple access (O-CDMA), pulse shaper.**

## I. Introduction

TIME-DIVISION multiplexing (TDM) and wavelength-division multiplexing (WDM) have been extensively explored and utilized in optical communication systems. Alternatively, optical-code-division multiple access (O-CDMA) is receiving increased attention due to its potential for enhanced information security, simplified and decentralized network control, improved spectral efficiency, and increased flexibility in the granularity of bandwidth that can be provisioned. In O-CDMA, different users whose signals may be overlapped both in time and frequency share a common communications medium; multiple access is achieved by assigning different, minimally interfering code sequences to different O-CDMA transmitters. In many O-CDMA approaches, as shown schematically in Fig. 1(a), input ultrashort pulses are time-spread during the encoding process into lower intensity noiselike signals [1]–[10]. In the receiver, data corresponding to a desired user is separated from multiaccess interference (MAI) via a matched filtering (decoding) operation, in which properly decoded signals are converted back to the original pulselike signals, while improperly decoded signals remain low-intensity, noiselike, temporally broadened waveforms. Multiuser, $\sim$ gigabits per second (Gb/s) O-CDMA systems have been demonstrated by several groups [3]–[8], including the authors' own previous demonstrations of four-user 2.5-Gb/s [3], [4] and 10-Gb/s [5], [6] O-CDMA systems utilizing reconfigurable spectral phase coding and low-power nonlinear waveform discrimination.

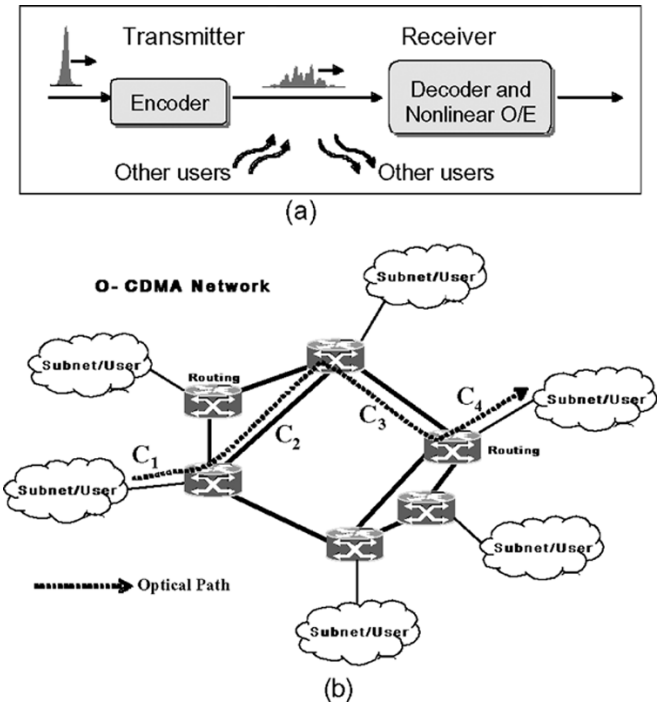


Fig. 1. (a) Conceptual diagram of an O-CDMA network. (b) Conceptual diagram of all-optical code translation in an O-CDMA network.

Code-division multiple access (CDMA) is well suited for network environments characterized by bursty data and multiple users, and O-CDMA provides the potential to use optical processing to perform certain network operations such as addressing and routing. Reconfigurable O-CDMA coding would allow the number of required codes to be reduced by code reallocation to share codes among subscribers, while all-optical code translation would enable the capability to form cascadable and/or routable O-CDMA networks (since modifying the code would be equivalent to modifying the address). Fig. 1(b) shows the conceptual diagram of code translation in an O-CDMA network. Suppose the signal encoded by code $C_1$ at a transmitter travels to the destination across one optical path, as shown in the figure. Since multiple users share the fiber transmission medium in O-CDMA networks, $C_1$ might have already been used between certain optical nodes due to the limited code space. If this does happen, code translation has to be employed to resolve the confliction. In this example, code $C_1$ is translated

Manuscript received August, 19 2004; revised December 14, 2004. The work on which this material was based was supported by the Defense Advanced Research Projects Agency (DARPA) under Grant MDA972-03-1-0014 and by the Air Force under Grant F49620-02-1-0240. The work of D. S. Seo was supported in part by the Korea Science and Engineering Foundation (KOSEF) under Grant R1-2003-000-10444-0 and by Inha University, Engineering Research Center (ERC), Korea, under Grant R11-2003-022-02002-0.

Z. Jiang, D. E. Leaird, and A. M. Weiner are with the School of Electrical and Computer Engineering, Purdue University, West Lafayette, IN 47907-2035 USA (e-mail: zjiang@purdue.edu).

D. S. Seo is with the School of Electrical and Computer Engineering, Purdue University, West Lafayette, IN 47907-2035 USA, on leave from the Department of Electronics, Myongji University, Kyonggido 449-728, Korea.

R. V. Roussev, C. Langrock, and M. M. Fejer are with Edward L. Ginzton Laboratory, Stanford University, Stanford, CA 94305-4088 USA.

Digital Object Identifier 10.1109/JLT.2005.849937

to $C_2$, $C_3$, and $C_4$, respectively, at the corresponding optical nodes along the optical path before reaching destination. As a result, code translation is an efficient way to increase user counts and/or reduce the number of required codes by reusing codes in O-CDMA networks. The ability to dynamically translate from one code to another in an O-CDMA network is analogous to dynamic wavelength conversion/switching, which is a key capability for reconfigurable wavelength-division-multiplexed (WDM) networks [11], [12].

Code translation in O-CDMA can be implemented via optoelectronic conversion (i.e., optical-to-electrical (O/E) or electrical-to-optical (E/O)) [13] while losing optical transparency. Previous efforts to pursue all-optical O-CDMA code translation have been reported in time-domain coding [14] and two-dimensional (2-D) time/wavelength coding [15]. Both of these efforts required a complicated nonlinear optical processing scheme with short code lengths (four to eight chips), and the code translators did not support dynamic reconfiguration. Moreover, the previous effort only demonstrated single-stage, single-user code translation. In this paper, reconfigurable all-optical code translation is demonstrated, for the first time to the authors' knowledge, in a spectrally phase coded O-CDMA testbed. Both one-stage and two-stage code translations induce less than 0.9-dB power penalties at each code translation. Multistage code translations (greater than two) are investigated via simulation and experimental emulation in a loop pulse shaper [22] to show the potential of code translations up to several tens of translations. In the proposed spectral phase coding scheme, the code translator is the same apparatus as the O-CDMA encoder/decoder and provides multistage code translation in a simple, linear, and delay-free scheme. Code translation is essentially instantaneous, limited only by the propagation time through the free-space apparatus, which is significantly faster than other methods based on optoelectronic conversion [13] or nonlinear optical processing in long fibers [14]. The programmability of the code translation function demonstrated here is a fundamental operation required for efficient reconfiguration of O-CDMA networks, which potentially shows better network performance than its fixed counterpart. Similar improvement was observed when using tunable, rather than fixed, wavelength conversion in WDM networks [11]. Furthermore, an interference user is included in the code translation demonstration so that the effect of MAI can be evaluated, which is a key issue in any O-CDMA demonstration.

Similar to previous O-CDMA all-optical code translation approaches [14], [15], all users will experience code translation in the proposed scheme. It is not possible to independently change the code for different users in the same fiber, which is similar to some of the wavelength conversion techniques in WDM networks. This is a constraint, for example, if only one user is expected to be code translated while keeping other users untouched. However, this could also be a significant advantage in some situations, analogous to simultaneous multiwavelength conversion in WDM networks [11], [12].

The remainder of this paper is structured as follows. In Section II, the theory of code translation is outlined. Section III presents the experimental and simulation result in four area: 1) one-stage code translation, 2) two-stage code translation, 3) pulse degradation caused by code translation, and 4) multistage code translation. The paper is concluded in Section IV.

## II. Principle of Code Translation

In our O-CDMA scheme, an input ultrashort pulse spectrum $A(\omega)$ is spectrally phase-coded as $A(\omega)\exp\{jC(\omega)\}$ and broadened to a pseudonoise waveform in the time domain, where $C(\omega)$ is the spectral phase code $C(\omega) = \{C_0(\omega_0), C_1(\omega_1), \ldots, C_{N-1}(\omega_{N-1})\}$. Here, $C_i(\omega_i)$ represents the $i$th spectral code chip in a code sequence of length $N$, which the encoder applies to a small band of frequencies centered at angular frequency $\omega_i$, $i = 0, 1, \ldots, (N-1)$. For $M$-ary phase coding, the phase in any particular chip is allowed to take on $M$ possible values, given by

$$C_i = \frac{2\pi k_i}{M}, \qquad k_i = 0, 1, \ldots, (M-1). \tag{1}$$

When $k_i = 0$ for all $C_i$ no phase modulation is applied, and the pulses remain uncoded.

Since the code translation devices are the same as encoder/decoder, all of them can be uniformly treated as coders for notation convenience. An optical path with $L$ coders consists of one encoder, $(L-2)$ code translators, and one decoder, corresponding to $(L-2)$-stage code translation. For proper decoding after passing through all of the stages, the accumulated spectral phase modulation for each code chip becomes equal to an integer multiple of $2\pi$, and the properly decoded waveform is converted back to a short pulse (the same temporal shape as the original input pulse); mathematically

$$\sum_{p=1}^{L} C^p = 0 \pmod{2\pi} \tag{2}$$

where $C^p$ is the phase code applied by the $p$th coder $p = 1, 2, \ldots, L$. Note that (2) represents a chip-by-chip summation, which can be broken into a set of $N$ equations explicitly

$$\sum_{p=1}^{L} C_i^p = 0 \pmod{2\pi}, \quad \text{for all } i = 0, 1, \ldots, (N-1) \tag{3}$$

where $C_i^p$ is the $i$th chip of phase code $C^p$ applied by the $p$th coder. In the special case of $L = 2$, it reduces to the familiar simple encoder/decoder pair without code translation, where codes for the encoder/decoder are conjugate when properly decoded.

On the other hand, at a translator knowing the incoming and outgoing waveforms with phase code $C^{\text{in}}$ and $C^{\text{out}}$, respectively, the code applied to code translator $C^T$ can be calculated as

$$C^T = C^{\text{out}} - C^{\text{in}} \pmod{2\pi}. \tag{4}$$

Again, (4) is based on chip-by-chip operation. Note that the code $C^{\text{out}}$ for an outgoing waveform differs from the code $C^T$ applied by the code translator. For successful code translation, the translated outgoing pseudonoise waveform with phase code $C^{\text{out}}$ shows distinct fine structure from the incoming waveform with phase code $C^{\text{in}}$.

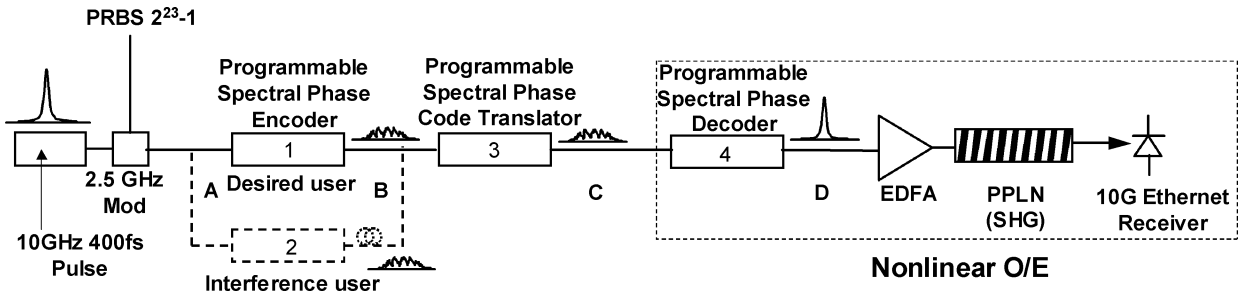


Fig. 2. Experimental apparatus for one-stage code translation.

CDMA systems typically utilize specific code families, where each code within the code family is known to exhibit desirable properties such as pseudorandom properties or low cross-correlation and autocorrelation sidelobes [10], [16]. Furthermore, many popular code families known from the communications literature are closed under summation in the sense that for any two member phase codes $C^a$ and $C^b$, the phase codes ($C^a \pm C^b$ modulo $2\pi$), which are formed via chip-by-chip operation, are also a member of the same code family. Examples of code families with good pseudorandom properties and that are closed under summation include $M$-sequences (a binary code $M = 2$) and the family $\mathcal{A}$ sequence (a quaternary code $M = 4$) [10], [16]. Therefore, in our scheme, not only do the codes exhibited by the coded waveforms along the optical path $(C^{\text{in}}, C^{\text{out}})$, but also all codes used by the encoder, translators, and decoder $(C^p, C^T)$ remain members of the original code family. These properties will be desirable for spectrally phase-coded O-CDMA networks, since they simplify the code translator design and configuration (essentially the same as encoder/decoder) and guarantee that the resultant MAI (improperly decoded) signal retains good pseudorandom properties. Both binary codes and quaternary codes from the communications literature have been used for successful system demonstrations in our previous literature [3], [4] and are suitable for application to code translation. The discussion of code translation also applies to orthogonal binary codes often used in O-CDMA system, e.g., Hadamard codes [6]. Hereafter, quaternary codes from the family $\mathcal{A}$ sequence ($M = 4$) are used unless otherwise specified.

## III. Results and Discussions

### A. One-Stage Code Translation Experiment

A schematic diagram of a single-stage O-CDMA code translation demonstration is shown in Fig. 2. An actively mode-locked fiber laser followed by a dispersion-decreasing fiber soliton compressor producing nearly transform-limited $\sim$ 0.4-ps pulses at $\sim$ 10 GHz centered near 1542 nm is used as the pulse source. A 2.5-Gb/s pseudorandom bit sequence (PRBS) $2^{23}-1$ data stream is impressed on the laser output with an intensity modulator (four pulses in each bit) and then split to generate both desired and interference users. For each user, the modulated ultrashort pulses are input into programmable spectral phase encoders—fiber-coupled Fourier transform pulse shapers [17]. User channels are independently controlled to equalize their powers and to obtain identical polarizations in order to correctly evaluate the effect of MAI. The output of each user path is decorrelated by a fiber-delay line and then combined at the programmable code translator—the third pulse shaper. The receiver [3], [4] consists of a decoder—the fourth pulse shaper—used to select the desired user to decode, an optical amplifier, a highly sensitive fiber-pigtailed periodically poled lithium niobate (PPLN) waveguide to perform the nonlinear discrimination function based on second-harmonic generation (SHG), and a 2.4-GHz-bandwidth photoreceiver, adapted from 10-Gb/s Ethernet, operating at the second-harmonic wavelength of 0.77 $\mu$m. Furthermore, appropriate lengths of dispersion-compensating fiber (DCF) are used to compensate the dispersion of the system. Only single-mode fiber (SMF) and DCF are used in our experiments; polarization-maintaining (PM) fiber is not employed.

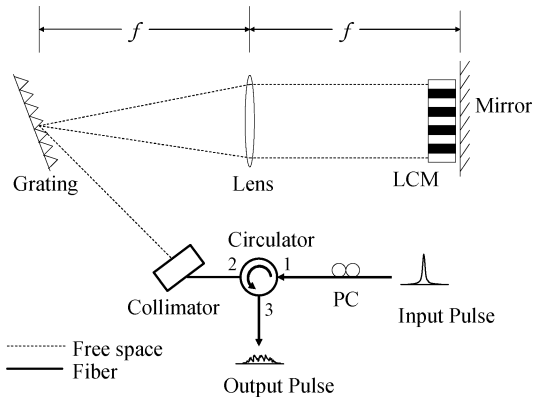


Fig. 3. Reflective pulse shaper used as encoder/translator/decoder. $f$: Focal length; PC: polarization controller; LCM: liquid-crystal modulator.

The encoder, decoder, and code translator are implemented by the well-developed ultrashort pulse-shaping techniques [17] using a fiber-coupled Fourier transform pulse shaper that incorporates a 128-element liquid-crystal modulator (LCM) array to spectrally phase-code the spectrum of the source laser. The individual pixels of the LCM can be electronically controlled independently to give an arbitrary phase shift in the range of 0 to $2\pi$ with 12-b resolution. The programmability of the LCM-array pulse shaper enables quick and convenient testing of various code families as well as the capability of reconfigurable code translation. Fig. 3 shows the reflective pulse shaper configuration used in our experiment [18]. Since the diffraction grating in our setup is polarization dependent, a polarization controller

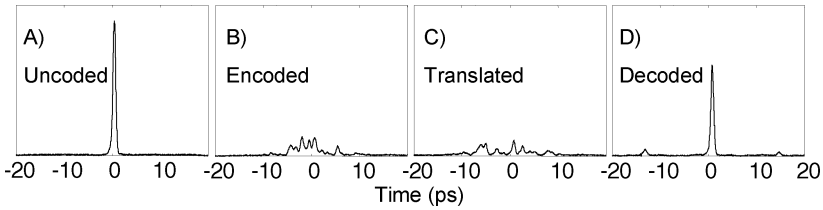


Fig. 4. Intensity cross-correlation measurements of the desired user: (a) uncoded, (b) encoded, (c) translated, and (d) properly decoded pulses.

(PC) is used before circulator port 1. A collimator is connected to circulator port 2. A telescope could be inserted after the collimator to magnify the beam size on the grating in order to enhance the spectral resolution, although that is not required in the current experiments. Discrete frequency components making up the input short pulse are diffracted by the grating and focused by the lens at the retroreflecting mirror. The LCM is placed just before the lens focal plane to enable programmable spectral phase coding. Special care has been taken by the LCM vendor to minimize the distance from the back of the apparatus housing to the liquid-crystal layer in order to minimize loss of resolution in the shaper. A retroreflecting mirror leads to a double-pass geometry, with all the frequencies recombined into a single fiber and with the output at circulator port 3. The pulse shaper is easily programmed under computer control, which allows reconfigurable encoding, decoding, and code translation. The fiber-to-fiber insertion loss of each pulse shaper is around 5 dB (including circulator loss). In our pulse shapers, the 12.8-mm aperture of the 128-pixel LCM array corresponds to a 17.9-nm wavelength range. Three of the pulse shapers have $\sim$ 200-$\mu$m resolution (resolution is defined as the focused beam diameter of any single optical frequency component at the LCM plane), corresponding to roughly two LCM pixels. The resolution of the fourth pulse shaper is $\sim$ 300 $\mu$m. All four pulse shapers support length-31 codes (four pixels per code chip), in which 124 pixels are used for coding while the unused four pixels are set to constant (zero) phase.

Fig. 4 shows intensity cross-correlation measurements of pulse waveforms for a desired user. A) in Fig. 4 shows the $\sim$ 0.4-ps uncoded pulse. B) shows the pulse after the encoder, which is broadened to an approximately 20-ps pseudonoise waveform resulting from spectral phase coding with a length-31 quaternary code from the family $\mathcal{A}$ sequence ($M = 4$, with phase shifts of 0, $\pi/2$, $\pi$, or $3\pi/2$) [16]. C) shows the pulse after the code translator, still a pseudonoise waveform but with distinctly different fine structure, which implies successful code translation. D) shows a properly decoded pulse after the decoder, where codes are selected to satisfy (2) so that the accumulated spectral phase modulation becomes zero (modulo $2\pi$). The properly decoded pulse is converted back to a short pulse with a small sidelobe due to coding degradation by the encoder/translator/decoder. A)–D) in Fig. 4 corresponds to the waveforms at points A–D in the experiment setup shown in Fig. 2. However, for experimental convenience, all of these waveforms are measured at the decoder output D by programming the unused, redundant pulse shapers to have a constant (zero) phase.

Fig. 5 shows the code-translated waveforms at the decoder output when both desired user and interference user

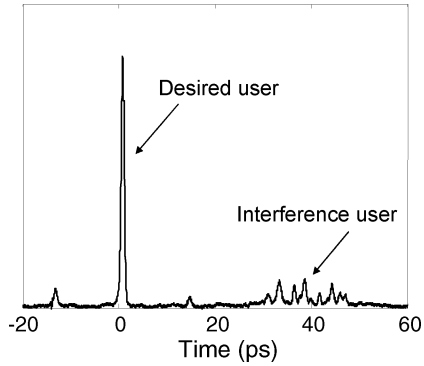


Fig. 5. Intensity cross-correlation measurements of both desired and interference users.

are selected. As expected, the properly decoded short pulse from a desired user and the improperly decoded low-intensity pseudonoise waveform from an interference user are clearly observed. The interference noise will be suppressed by the following nonlinear optical processing in the O-CDMA system testbed. Note that a slot-level timing coordination scheme is applied to separate the desired user and interference user by $\sim$ 40 ps to avoid beat noise caused by their interaction [3]–[5]. An ideal O-CDMA is well suited for bursty network environments, and the asynchronous nature of data transmission can simplify and decentralize network management and control. However, full asynchronism is difficult to implement for O-CDMA in practice while simultaneously maintaining sufficient MAI suppression. Therefore, some level of synchronism is built into many $\geq$ two-user O-CDMA schemes. To suppress MAI effectively, many O-CDMA systems have relied on precise timing coordination at the transmitter, with coordination/synchronism required at the level of the finest feature in the coded waveforms, equal to the duration of uncoded or properly decoded pulses, typically on the order of $\sim$ picoseconds [6]–[9]. This is referred to as chip-level timing coordination. Prior work in our group demonstrated a four-user, 2.5-Gb/s, and 10-Gb/s spectrally phase-coded O-CDMA system with strong nonlinear interference suppression, without the need for chip-level timing coordination at the transmitter [3]–[5]. In our system, slot-level timing coordination was used to relax timing constraints: each bit period was divided into multiple time slots (equal to or longer than the coded waveform duration, which is much longer than the chip duration), with each user assigned to a different time slot. System performance was degraded due to beat noise as the time-slot duration was decreased below the coded waveform duration, which limited the available time slots and users [4], [5]. A comprehensive discussion of different timing scheme in ultrashort-pulse O-CDMA is given in [4].

Degradation caused by beat noise is a universal problem for multiuser O-CDMA systems. In general, increasing timing coordination and synchronism can provide greater user counts and better performance, at the cost of greater complexity [6]–[9]. We also demonstrated an O-CDMA system with hybrid-chip- and slot-level timing coordination, showing the potential of higher total user counts with both multiple users per slot and multiple slots [6]. In our current code translation demonstration, to focus on the code translation functionality, we adopt the relatively simple slot-level timing coordination scheme to illustrate the MAI effect, i.e., the desired user and interference user are separated to maintain sufficient MAI suppression.

In order to correctly recover data at the receiver, data corresponding to a desired user has to be separated from MAI after decoding. Since the energy in properly and improperly decoded pulses is similar, and since the temporal duration of even improperly decoded pulses is on the order of the bit period or below, both properly and improperly decoded pulses will appear identical to an electronic receiver band-limited to the data rate. Consequently, either very fast electronics or a nonlinear optical intensity discriminator play a critical role in separating properly decoded short pulses from improperly decoded MAI. In our experiment, an ultrasensitive nonlinear optical intensity discriminator based on SHG in a PPLN waveguide is used [19], [20]. The measured SHG efficiency of the PPLN waveguide is 3.1%/mW for continuous wave (CW) and 170%/pJ for ultrashort pulses. Our discriminator permits MAI suppression as high as 20 dB [19] and has been demonstrated in a four-user, 10-Gb/s system operating at an energy of $\sim$ 30 fJ/b [5], as much as two orders lower than discriminators based on nonlinear fiber optics [2], [8]. The ability to operate at low power per user is critical for scaling O-CDMA to greater numbers of users. In multiuser networking, each receiver will see a sample of each of the multiple-access signals; therefore, the required amplifier saturation power scales with the number of users (as well as bit rate) [2], [3]. Further, full interference suppression was realized without the need for synchronous detection due to the nonlinear processing property, which significantly simplifies system control.

Fig. 6 shows eye diagrams and the corresponding bit-error-rate (BER) curves versus total power in the nonlinear discriminator. The results without code translation are obtained by programming the code translator to have a constant phase; the desired user is still properly decoded by the appropriate code choice at the decoder. To demonstrate effective MAI suppression, results for single-user operation are also presented for comparison. In both situations, code translation induces less than 0.6-dB power penalty, which we attribute to coding degradation added by the code translator. Small power penalties point out the feasibility of multistage code translation. The 3.5-dB power difference between single-user and two-user BER curves indicates 0.5-dB power penalty caused by MAI since a 3-dB power difference is simply due to the doubling of the number of users at the nonlinear discriminator. We attribute this 0.5-dB power penalty to the finite interference suppression of the nonlinear discriminator. The power requirement of less than $-3$ dBm per user at BER $= 10^{-9}$ provides substantial margin for scaling to higher bit rates and larger user counts.

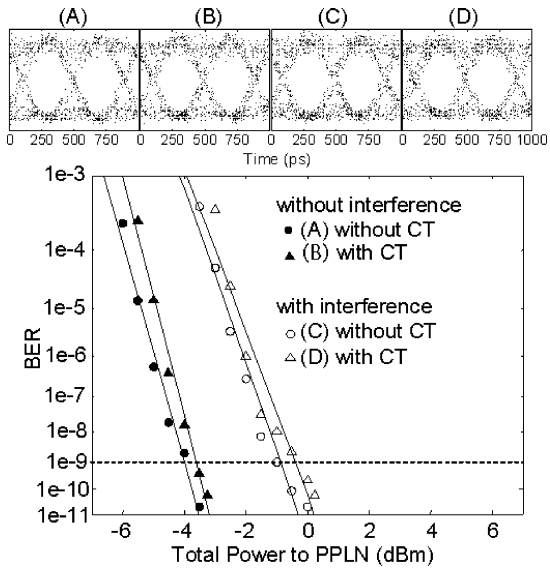


Fig. 6. Eye diagrams and BER measurements of (A) a single user without code translation (CT), (B) a single user with CT, (C) two users without CT, and (D) two users with CT.

### *B. Two-Stage Code Translation Experiment*

Fig. 7 shows the experimental apparatus for two-stage code translation, which is similar to the previous one-stage code translation. One more pulse shaper is added as the second code translator. The desired user is combined with an uncoded pulse interference user [3], [4] after the first stage code translation. As a result, the desired user and the interference user experience different code translation paths and number of translation times emulating what would happen in an actual network environment. One more optical amplifier is added for loss compensation.

Fig. 8(a) shows intensity cross-correlation measurements of pulse waveforms for the desired user: A) uncoded, B) encoded, C) translated once, D) translated twice, and E) properly decoded pulses. Fig. 8(b) shows the length-31 quaternary phase codes applied to the encoder, code translator 1, code translator 2, and decoder. Translated pulses remain pseudonoise waveforms but with distinct fine temporal structures. The pseudonoise waveforms that are encoded and translated once are different from the previous single-stage translation experiment because different quaternary codes are applied. The properly decoded pulse is converted back to a short pulse, demonstrating successful two-stage code translation and decoding. Again, A)–E) in Fig. 8(a) correspond to waveforms at points A–E, as shown in the experimental setup of Fig. 7, but all waveforms are measured at point E by programming unused pulse shapers to have a constant phase, as we did previously. Again, the desired user and interference user are separated by $\sim$ 40 ps (not shown).

Fig. 9 shows BER curves for two-stage code translation. The results without code translation are obtained by programming both code translators to have a constant phase. The results with code translation once (not from previous one-stage experiment) are obtained by programming the code translator 2 to have a constant phase. The desired user is still properly decoded by

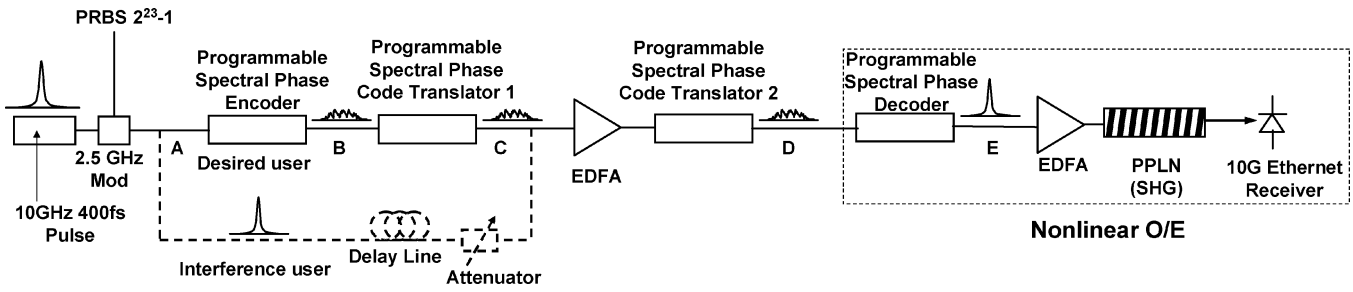


Fig. 7. Experimental apparatus for two-stage code translation.

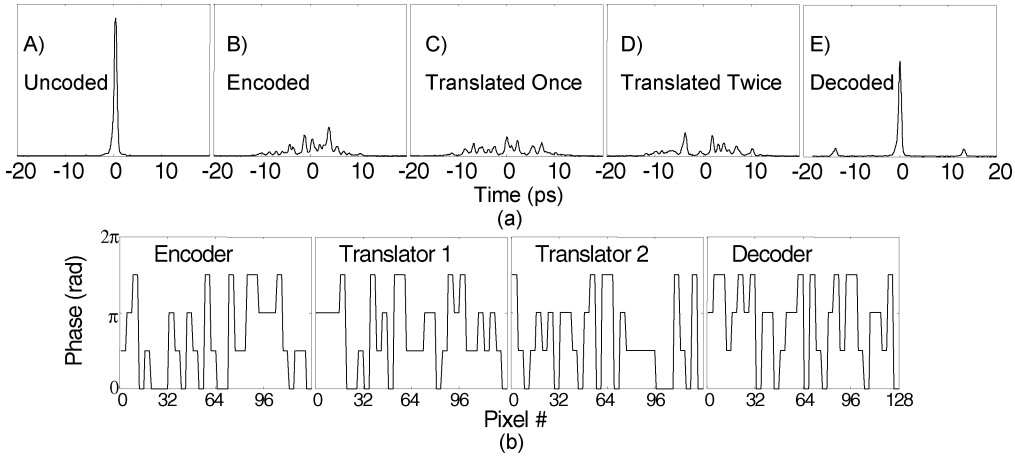


Fig. 8. (a) Intensity cross-correlation measurements of the desired user: A) uncoded, B) encoded, C) translated once, D) translated twice, and E) properly decoded pulses. (b) Length-31 quaternary phase codes applied to encoder, code translator 1, code translator 2, and decoder.

choosing appropriate codes at the decoder for both cases. To demonstrate effective MAI suppression, results for a single user (without interference) are also shown for comparison. In both situations, less than a 0.9-dB power penalty is observed at each code translation. Again, the power requirement of less than $-3$ dBm per user at BER $= 10^{-9}$ provides substantial margin for scaling to higher bit rates and larger user counts. Fig. 9 shows better BER performance for a single user (in the absence of interference) compared with the one-stage translation experiment in Fig. 6, which may be attributed to better dispersion compensation in the two-stage translation experiment. On the other hand, results for two users show similar performance, possibly because the interference user is only present in one code translation stage and therefore experiences less coding loss than the desired user. Thus, compared with the one-stage translation experiment, the ratio of interference to desired user should be somewhat larger in the two-stage translation experiment.

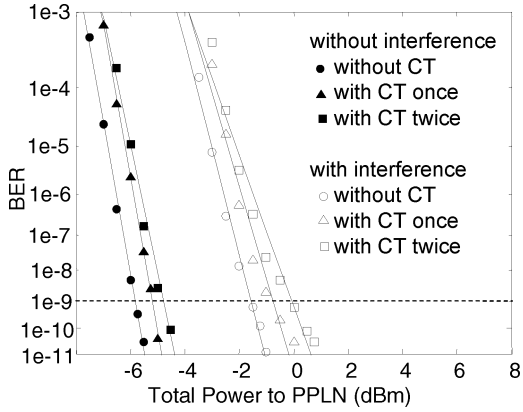


Fig. 9. BER measurements of two-stage code translation for single user and two users. CT: Code translation.

### C. Pulse Degradation Caused by Coding

According to the pulse intensity cross-correlation measurement, a properly decoded pulse is converted back to a short pulse but is degraded with small sidelobes and reduced in peak intensity. In this section, pulse degradation caused by the coding process is investigated in detail based on experiment and simulation.

We use the same two-stage code translation experimental setup shown in Fig. 7 with four cascaded pulse shapers (without an interference user). Fig. 10(a) shows the intensity cross-correlation measurement for a properly decoded pulse after a different number of coding operations. An appropriate quaternary code combination is applied to enable proper decoding for each case. All of the pulses are measured at point E, while unused pulse shapers are set to have a constant phase: A—zero coding operations—all of the four pulse shapers are set to a constant phase corresponding to an uncoded pulse; B—two coding operations (encoder to decoder)—code translator 1 and 2 shapers are set to a constant phase corresponding to a properly decoded pulse by the encoder–decoder pair; C—three coding operations (encoder to translator one to decoder)—the code

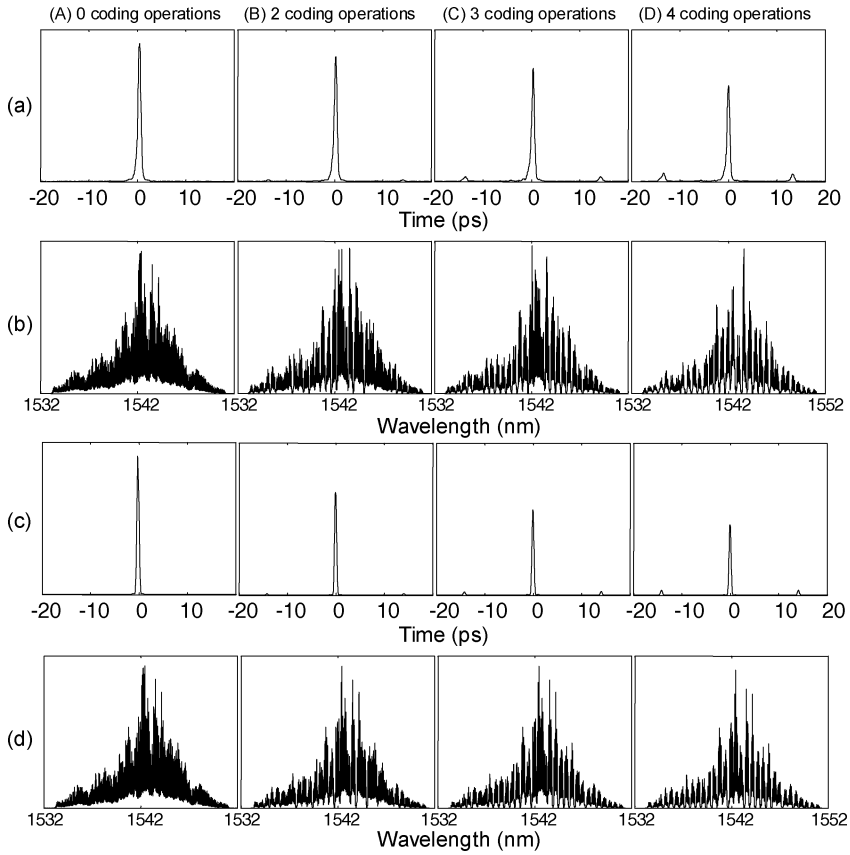


Fig. 10. Decoded pulse degradation caused by (A) zero coding operations (uncoded pulse), (B) two coding operations, (C) three coding operations, and (D) four coding operations. (a) Intensity cross-correlation measurements. (b) Spectral measurements. (c) Simulation of pulse intensities. (d) Simulation of spectra (uncoded spectrum is taken from experiment).

translator 2 shaper is set to a constant phase corresponding to single-stage code translation; and D—four coding operations (encoder to translator one to translator two to decoder) corresponding to two-stage code translation. Note that we need at least two shapers (encoder and decoder) to recover the original short pulse. From this data, it is clear that pulse degradation increases with the number of coding operations, showing lower peak intensity and larger sidelobes. Pulse degradation is mainly due to the spectral phase coding process in encoder/translators/decoder. Fig. 10(b) shows the measured optical spectra corresponding to the time-domain traces shown in Fig. 10(a). The spectrum for the uncoded pulse (A) shows $\sim$ 17.9-nm spectral coding range across the 128 LCM pixels. Clear spectral dips are observed in the spectra of (B)–(D) whenever a phase transition (0, $\pi/2$, $\pi$, or $3\pi/2$) occurs in the spectrum, which explains the pulse degradation, including coding loss, sidelobes, and slight pulse broadening. In this example, after four coding operations (two-stage code translation), all 31 spectral dips occur for length-31 quaternary codes. If a phase transition occurs at the position of an already existing dip, the spectral dip becomes wider and deeper. Therefore, as the number of coding operations increases, the number of spectral dips increases and/or the dips become wider and deeper. The spectral dips result from diffraction effects arising from the frequency components falling at phase transition regions of the LCM in the pulse shaper, which has been quantitatively clarified previously [2], [21].

As mentioned previously, we attribute the pulse degradation to spectral dips caused by the diffraction effects. Simulation is performed to confirm this argument based on the theoretical model in [2] and [21]. Only the spectral phase coding effect is considered in our simulation. The measured uncoded spectrum [(A) in Fig. 10(b)] is used as the input spectrum (assume no initial spectral phase) to our simulation. The measured pulse shaper resolutions are used in the simulation: 300-$\mu$m resolution for translator 2 and 200-$\mu$m resolution for the other three pulse shapers. Fig. 10(c) and (d) shows the simulation results of pulse intensities and spectra corresponding to Fig. 10(a) and (b). The spectral dips are in excellent agreement with the experimental results. Pulse peak intensity reduction and sidelobe appearance are consistent with experiments. Pulsewidths of simulations are narrower than those of experiments because experimental measurements yield pulse intensity cross correlation instead of intensity itself. More noticeably, peak intensities of simulations are lower than those of experiments where coding losses are partially compensated by optical amplifiers operated in the saturation regime, an effect that is not considered in our simulation. This also explains why the decoded pulse peak intensity in the single-stage translation experiment [(D) in Fig. 4] is lower than the result shown in (C) in Fig. 10(a) since one more optical amplifier is used in the setup. The details of the sidelobes after four coding operations are investigated through both experiment and simulation, as shown in Fig. 11, where a second-order sidelobe arises. The intensity scales are adjusted for easy comparison.

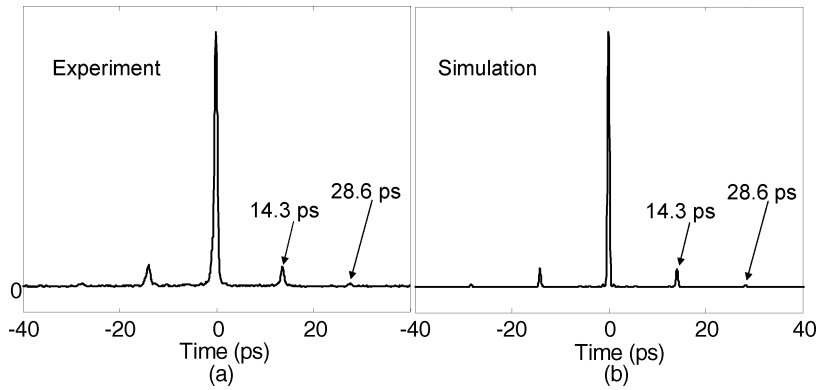


Fig. 11. Sidelobe of decoded pulses after four coding operations. (a) Intensity cross-correlation measurement. (b) Simulation of pulse intensity.

First-order and second-order sidelobes are located at $\pm 14.3$ and $\pm 28.6$ ps, respectively. The sidelobe positions and relative amplitudes agree well between simulation and experiment. The positions of sidelobes can also be calculated in a simple way: each code chip occupies a bandwidth of $17.9/128 \times 4 = 0.56$ nm (69.9 GHz), which is the inverse of the position of the first-order sidelobe at 14.3 ps.

To quantify further the comparison between experiment and simulation, we first calculate the normalized peak intensity of a properly decoded pulse versus the number of coding operations, as shown in Fig. 12. As mentioned previously, experimental peak intensities are higher than simulation because the coding loss is partially compensated by optical amplifiers working in saturation regime. Since the pulse peak intensity reduction can be compensated by optical amplifiers, it may not be a good indicator of pulse degradation. On the other hand, the agreement of sidelobes between experiment and simulation in Fig. 11 prompts us to characterize pulse degradation using the sidelobes. Fig. 12 also shows the ratios of sidelobe (first-order) energy to total pulse energy, which are not affected by optical amplifiers. The sidelobe energies are measured and calculated by integrating the sidelobes of the waveforms. The experimental results agree well with simulations considering experimental uncertainties.

This discussion has centered on desired user (properly decoded short pulse) degradation caused by code translation. A closely related issue is the effect on the interference user (improperly decoded pseudonoise waveform) or users of passing through the code translators. After code translation, the interference user is coded by another code, with almost the same characteristics as the originally encoded (broadened pseudonoise) waveform. The only difference is that there are more spectral dips (and/or wider and deeper dips) caused by code translation, similar to what is experienced by the desired user after code translation. Such spectral dips on the interference user are associated with loss, which reduces the MAI power in the system. Although the spectral dips may also introduce some distortion onto broadened pseudonoise (MAI) waveforms, such slight distortion is not expected to significantly affect the suppression of improperly decoded pseudonoise signals at the receiver/nonlinear discriminator. Overall, with an increasing number of spectral dips and loss onto the interference user, there should be a slight benefit (rather than a negative effect) to O-CDMA system operation,

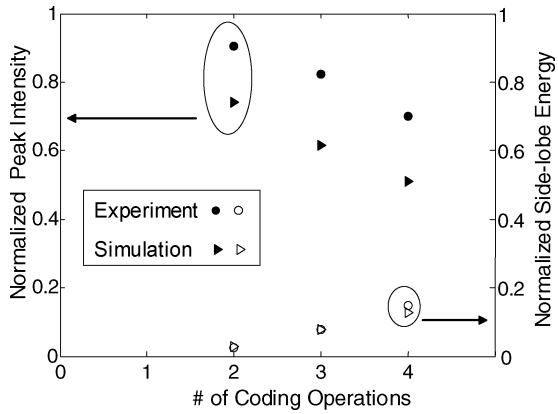


Fig. 12. Comparison of experiment and simulation of pulse degradation caused by multiple coding operations (equivalently code translation): normalized peak intensity (filled symbols) and sidelobe energy (open symbols).

since the MAI power becomes smaller. On the other hand, for the desired user, the spectral dip effect caused by code translation has a negative impact on system performance, as discussed in previous paragraphs. Overall, we believe that the degradation effect on the desired user due to passing through the code translators is more important than the effect of such translation on the MAI. Therfore, we have focused our attention in this paper on the effects of such degradation on the desired user. This is a conservative approach, since the effects we are ignoring, i.e., the reduction in MAI power, would be expected to mitigate in part the reduction in desired user intensity.

### *D. Multi-Stage Code Translation*

*1) Simulation of Multistage Code Translation:* As we have observed in an experimental example, after four coding operations (two-stage code translation), all 31 spectral dips occur for length-31 quaternary codes (one dip comes from the spectral phase change between coded pixels and the unused four pixels). We may expect that pulse degradation will show saturation behavior in multistage code translation with a large number of coding operations since all dips already occur after the first few coding operations (although spectral dips become wider and deeper during additional coding operations). We first quantitatively investigate multistage code translation through simulation in the same way as we did in the previous section. Fig. 13(a) shows normalized peak intensity of a properly decoded pulse

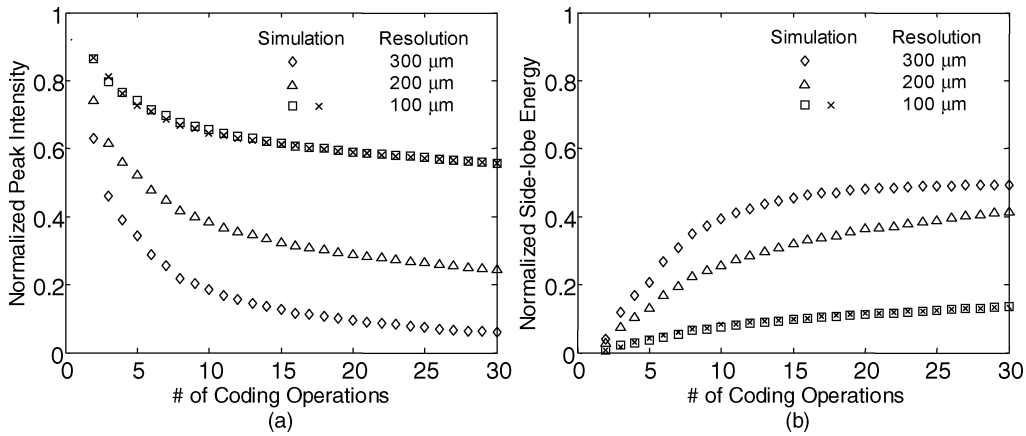


Fig. 13. Pulse degradation caused by multistage code translation: (a) normalized peak intensity and (b) normalized sidelobe energy. Two examples using different sets of quaternary codes are presented for 100-$\mu$m resolution.

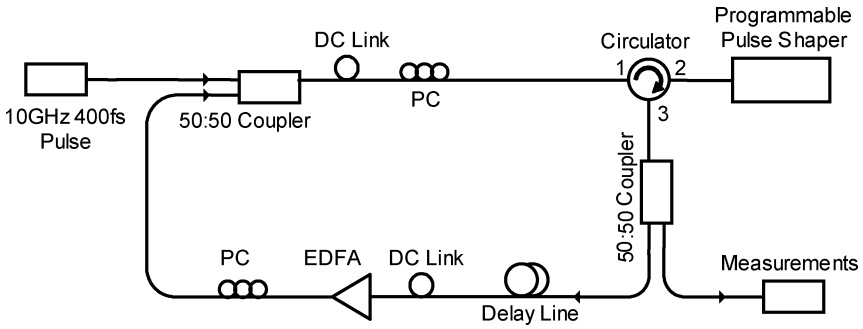


Fig. 14. Experimental apparatus for multistage code translation emulation: Pulse shaper in a loop. PC: Polarization controller. DC: Dispersion-compensating fiber.

versus the number of coding operations. All pulse shapers have identical resolution, in which 100-, 200-, or 300-$\mu$m resolutions are used in the calculations, respectively. A larger reduction of pulse peak intensity occurs for the first few coding operations, but less reduction happens for additional coding operations as predicted by qualitative analysis. Pulse peak intensity reduction largely depends on the shaper resolution, which is reduced to 6.0% of the peak value after 30 coding operations for 300-$\mu$m resolution but improved to 56.0% of the peak value for 100-$\mu$m resolution. Specific codes applied to all shapers also affect simulation results. Two examples are presented for 100-$\mu$m resolution using two sets of quaternary codes, which only shows a slight difference and essentially the same profile. Fig. 13(b) shows the ratio of sidelobe (first-order) energy to total pulse energy. Again, degradation saturation behavior is observed. Sidelobe energy also largely depends on the shaper resolution, which reaches 49.3% of total pulse energy after 30 coding operations for 300-$\mu$m resolution but is only 13.5% of total pulse energy for 100-$\mu$m resolution. On the other hand, note that we have achieved satisfactory system performance under a similar degradation condition in the two-stage code translation experiment where the sidelobe energy is 14.7% of total pulse energy, as shown in Fig. 12. As a result, the agreement between our experiment and simulation for one- and two-stage code translation, together with simulation for multistage code translation, shows the potential of several tens of code translations utilizing high-resolution pulse shapers.

*2) Experimental Emulation of Multistage Code Translation: Pulse Shaper in a Loop:* To emulate multistage code translations without the need for a large number of pulse shapers, we proposed a scheme to emulate this process—a pulse shaper in a closed loop where a portion of the shaper output is fed back to the input so as to experience multiple passes through the shaper [22], as shown in Fig. 14. This loop scheme allows testing of the multistage code translation process in a simple and convenient setup. In actual O-CDMA networking applications, code translation would instead take place in distinct pulse shapers located at different nodes as demonstrated in the previous sections. The same laser source described previously is used, and all fiber links are dispersion compensated using an appropriate combination of SMF and DCF. A reflective pulse shaper is inserted into the closed loop to permit multiple coding. After the pulse shaper, a portion of the coded output is amplified by an optical amplifier and reinjected into the shaper through the input coupler.

For the pulse shaper in a loop, code $C^o$ is imposed onto the spectrum during each of $n$ passes through the shaper. Therefore, the output waveform after $n$ passes corresponds to another spectral phase code $nC^o$ due to the identical code in all $n$ passes. Whenever the accumulated spectral phase modulation for each code chip becomes equal to an integer multiple of $2\pi$, the pulse shaper produces a properly decoded pulse (same temporal shape as the original input pulse) so that mathematically

$$nC^o = 0 \pmod{2\pi}. \tag{5}$$

Similar to (2), (5) is based on chip-by-chip operation. Actually, (5) is a special case of (2), where $L = n$ and identical code $C^o$ is used by all coders. For $M$-ary phase coding, where the phase in any particular chip is allowed to take on $M$ possible values given by (1), (5) is satisfied whenever $n$ is an integer multiple of $M$. When the number of passes $n$ is not equal to a multiple of $M$, according to the number of passes $n$ modulo $M$, the pulse shaper output corresponds to a set of $(M-1)$ distinct pseudonoise waveforms, indicating multiple code-translated waveforms.

Fig. 15 shows intensity cross-correlation measurements of the output of the closed-loop pulse shaper. The numbers labeling the pulses represent the number of passes ($n$) through the shaper. The delay through the loop is fine-tuned using a fiber stretcher to give an apparent advancement of approximately 15 ps per pass (relative to the 100-ps periodicity arising from the 10-GHz laser repetition rate). For no phase coding (the shaper is set at a constant phase), exponentially decaying pulse trains (with essentially identical shape) are observed, as shown in Fig. 15(a). The attenuation corresponds to a net loop loss of $\sim$ 3 dB per pass. The peaks corresponding to the first eight passes through the pulse shaper are visible. Since only one pulse shaper (thus, one code) is used in the closed loop, it is not feasible to properly decode the pulse using a combination of distinct codes in the loop shaper for multistage code translation, as demonstrated in the previous section. However, note that it is still a valid code translation demonstration even if all pulse shapers use one identical code because each translated pulse exhibits distinct waveforms and represents a distinct code. To illustrate this sort of code translation using one identical code in loop shaper, we incorporate two-level ($M = 2$, binary) and three-level ($M = 3$) codes as well as the four-level ($M = 4$, quaternary) code used previously. Length-31 code chips are used for all three cases. For a two-level (0, $\pi$) $M$-sequence code, the output pulses are broad noiselike waveforms after odd numbers of passes, while they are decoded back to their original shape after even numbers of passes, as shown in Fig. 15(b). Three complete encoding–decoding cycles can be observed. This clearly demonstrates the cascadable nature of the encoding–decoding process. Although for the two-level code, one may consider the experiment as cascaded identical encoding/decoding operations rather than code translation; the capability to properly decode back to a short pulse after six shaper passes is still demonstrated. To some extent, this could be considered as a generalized four-stage code translation if the all-zero ($\mathrm{mod}\ 2\pi$) spectral phase code is also treated as a code. Fig. 15(c) shows results obtained using a three-level (0, $2\pi/3$, and $4\pi/3$) code where the phases of each chip are randomly selected. Two distinct encoded waveforms appear at the delay positions corresponding to $n = 1$, 4 and to $n = 2$, 5, respectively, while decoded short pulses appear at $n = 3$, 6. This corresponds to two cycles of one-stage code translation using one identical code. Or similar to (b), this could be considered as a generalized four-stage code translation. For a four-level (0, $\pi/2$, $\pi$, and $3\pi/2$) code, three different encoded waveforms are observed before the pulse is successfully decoded, as shown in Fig. 15(d), which corresponds to a two-stage code translation using one identical code. These results show that a pulse could be properly decoded after going through as many as six pulse shapers (loop loss and 100-ps periodicity limit us from detecting more), proving the feasibility of multistage code translation application. The fundamental limitation of the number of code translation comes from the coding degradation as investigated previously; nevertheless, several tens of code translations should be possible, as shown in our simulation results.

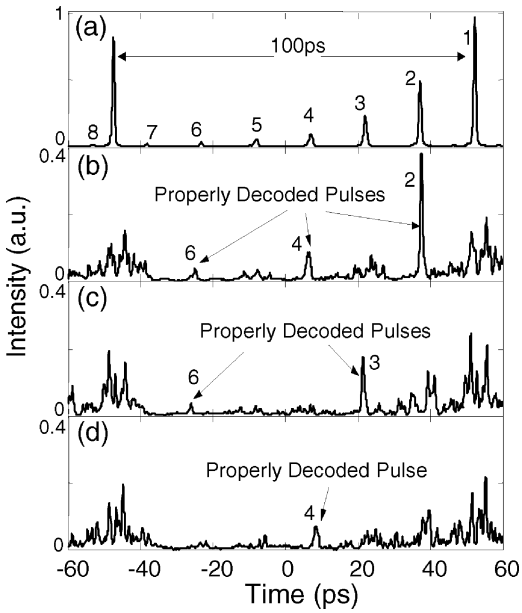


Fig. 15. Intensity cross-correlation measurements of multistage code translation emulation. The numbers labeling the pulses represent the number of shaper passes.

## IV. Discussion and Conclusion

In an all-optical code translation scheme, all users will experience code translation. This could be a significant advantage, analogous to multiwavelength conversion in wavelength-division-multiplexed (WDM) networks [11], [12]. In certain network applications, it is desirable that only one user is expected to be code translated while keeping other users untouched. In such a situation, the target user has to be separated from other users, translated to a new code, and inserted back to the network, which is a combination of add–drop and code translation functionalities in an optical-code-division multiple-access (O-CDMA) network. An asynchronous add–drop scheme has been proposed [23] for ultrashort-pulse spectrally phase-coded O-CDMA, but its implementation still remains a challenge.

In summary, reconfigurable all-optical code translation has been experimentally demonstrated in a spectrally phase-coded O-CDMA testbed with an included interference user. Both one-stage and two-stage code translations induce less than a 0.9-dB power penalty for each code translation. Multistage code translations are investigated via simulation and experimental emulation in a loop pulse shaper, showing the potential of up to several tens of code translations. Pulse degradation caused by the coding process is studied theoretically through simulation and confirmed by experiments. The key result, namely demonstration of high-quality code translation, is possible due

to the properties of spectral phase coding. In the proposed spectral phase-coding scheme, the code translator is the same as the O-CDMA encoder/decoder and provides multistage code translation in a simple, linear, and delay-free scheme. The programmability of the code translation function demonstrated here is a fundamental operation required for reconfigurable O-CDMA networks, suggesting the possibility of addressing and routing in O-CDMA networks based on all-optical code translation.

## REFERENCES


[1] J. A. Salehi, A. M. Weiner, and J. P. Heritage, "Coherent ultrashort light pulse code-division multiple access communication systems," *J. Lightw. Technol.*, vol. 8, no. 3, pp. 478–491, Mar. 1990.

[2] H. P. Sardesai, C. C. Chang, and A. M. Weiner, "A femtosecond code-division multiple access communication system test bed," *J. Lightw. Technol.*, vol. 16, no. 11, pp. 1953–1964, Nov. 1998.

[3] Z. Jiang, D. S. Seo, S.-D. Yang, D. E. Leaird, A. M. Weiner, R. V. Roussev, C. Langrock, and M. M. Fejer, "Four user, 2.5 Gb/s, spectrally coded O-CDMA system demonstration using low power nonlinear processing," presented at the 2004 Optical Fiber Conf. (OFC 2004), Los Angeles, CA, 2004, Postdeadline Paper PDP29.

[4] ——, "Four user, 2.5 Gb/s, spectrally coded O-CDMA system demonstration using low power nonlinear processing," *J. Lightw. Technol.*, vol. 23, no. 1, pp. 143–158, Jan. 2005.

[5] ——, "Four user, 10 Gb/s spectrally phase coded O-CDMA system operating at $\sim$ 30 fJ/bit," *IEEE Photon. Technol. Lett.*, vol. 17, no. 3, pp. 705–707, Mar. 2005.

[6] Z. Jiang, D. S. Seo, D. E. Leaird, A. M. Weiner, R. V. Roussev, C. Langrock, and M. M. Fejer, "Multi-user, 10 Gb/s spectrally phase coded O-CDMA system with hybrid chip and slot-level timing coordination," *IEICE Electron. Express*, vol. 1, pp. 398–403, Oct. 2004.

[7] H. Sotobayashi, W. Chujo, and K. Kitayama, "Highly spectral-efficient optical code-division multiplexing transmission system," *IEEE J. Sel. Topics Quantum Electron.*, vol. 10, no. 2, pp. 250–258, Mar./Apr. 2004.

[8] R. P. Scott, W. Cong, K. Li, V. J. Hernandez, B. H. Kolner, J. P. Heritage, and S. J. B. Yoo, "Demonstration of an error-free $4 \times 10$ Gb/s multiuser SPECTS O-CDMA network testbed," *IEEE Photon. Technol. Lett.*, vol. 16, no. 9, pp. 2186–2188, Sep. 2004.

[9] S. Etemad, T. Banwell, S. Galli, J. Jackel, R. Menendez, P. Toliver, J. Young, P. Delfyett, C. Price, and T. Turpin, "Optical-CDMA incorporating phase coding of coherent frequency bins: Concept, simulation, experiment," presented at the 2004 Optical Fiber Conf. (OFC 2004), Los Angeles, CA, 2004, Paper FG5.

[10] P. C. Teh, M. Ibsen, J. H. Lee, P. Petropoulos, and D. J. Richardson, "Demonstration of a four-channel WDM/OCDMA system using 255-chip 320-Gchip/s quaternary phase coding gratings," *IEEE Photon. Technol. Lett.*, vol. 14, no. 2, pp. 227–229, Feb. 2002.

[11] R. Ramaswami and K. N. Sivarajan, *Optical Networks: A Practical Perspective*. San Francisco, CA: Morgan Kaufmann, 1998.

[12] S. J. B. Yoo, "Wavelength conversion technologies for WDM network applications," *J. Lightw. Technol.*, vol. 14, no. 6, pp. 955–966, Jun. 1996.

[13] K. Kitayama, "Code division multiplexing lightwave networks based upon optical code conversion," *IEEE Sel. Areas Commun.*, vol. 16, no. 9, pp. 1309–1319, Sep. 1998.

[14] K. Kitayama, N. Wada, and H. Sotobayashi, "Architectural considerations for photonic IP router based upon optical code correlation," *J. Lightw. Technol.*, vol. 18, no. 12, pp. 1834–1844, Dec. 2000.

[15] D. Gurkan, S. Kumar, A. Sahin, A. Willner, K. Parameswaran, M. Fejer, D. Starodubov, J. Bannister, P. Kamath, and J. Touch, "All-optical wavelength and time 2-D code converter for dynamically-reconfigurable O-CDMA networks using a PPLN waveguide," presented at the 2003 Optical Fiber Conf. (OFC 2003), Atlanta, GA, 2003, Paper FD6.

[16] S. Boztas, R. Hammons, and P. V. Kumar, "4-phase sequences with near-optimum correlation properties," *IEEE Trans. Inf. Theory*, vol. 38, no. 3, pp. 1101–1113, May 1992.

[17] A. M. Weiner, "Femtosecond pulse shaping using spatial light modulators," *Rev. Sci. Instrum.*, vol. 71, pp. 1929–1960, May 2000.

[18] R. D. Nelson, D. E. Leaird, and A. M. Weiner, "Programmable polarization-independent spectral phase compensation and pulse shaping," *Opt. Express*, vol. 11, pp. 1763–1769, Jul. 2003.

[19] Z. Jiang, D. S. Seo, S.-D. Yang, D. E. Leaird, A. M. Weiner, R. V. Roussev, C. Langrock, and M. M. Fejer, "Low power, high-contrast, coded waveform discrimination at 10 GHz via nonlinear processing," *IEEE Photon. Technol. Lett.*, vol. 16, no. 7, pp. 1778–1780, Jul. 2004.

[20] Z. Zheng, A. M. Weiner, K. R. Parameswaran, M. H. Chou, and M. M. Fejer, "Low-power spectral phase correlator using periodically poled $LiNbO_3$ waveguides," *IEEE Photon. Technol. Lett.*, vol. 13, no. 4, pp. 376–378, Apr. 2001.

[21] R. N. Thurston, J. P. Heritage, A. M. Weiner, and W. J. Tomlinson, "Analysis of picosecond pulse shape synthesis by spectral masking in a grating pulse compressor," *IEEE J. Quantum. Electron.*, vol. 22, no. 5, pp. 682–696, May 1986.

[22] D. S. Seo, Z. Jiang, D. E. Leaird, and A. M. Weiner, "Pulse shaper in a loop: Demonstration of cascadable ultrafast all-optical code-translation," *Opt. Lett.*, vol. 29, pp. 1864–1866, Aug. 2004.

[23] Z. Zheng, A. M. Weiner, K. R. Parameswaran, M. H. Chou, and M. M. Fejer, "Femtosecond second harmonic generation in periodically poled lithium niobate waveguides with simultaneous strong pump depletion and group-velocity walk-off," *J. Opt. Soc. Amer. B, Opt. Phys.*, vol. 19, pp. 839–848, Apr. 2002.


**Z. Jiang** (S'03) received the B.S. (with highest honors) and the M.S. degrees, both from the Department of Electronics Engineering, Tsinghua University, Beijing, China, in 1999 and 2002, respectively. He is now working toward the Ph.D. degree at the School of Electrical and Computer Engineering, Purdue University, West Lafayette, IN.

His research focuses on the areas of ultrafast technology, optical pulse shaping, optical fiber communication, and fiber nonlinearity. He has been author or coauthor of more than 30 journal articles and conference papers.

Mr. Jiang was awarded the Ross and Mary I. Williams Fellowship Award from Purdue University (2002–2003). He has been selected as a finalist for the 2005 Optical Society of America (OSA) New Focus/Bookham Student Award. He is also an active reviewer for the IEEE PHOTONICS TECHNOLOGY LETTERS and the JOURNAL OF LIGHTWAVE TECHNOLOGY.

**D. S. Seo** (M'00) received the B.S. and M.S. degrees in electronic engineering from Yonsei University, Korea, in 1980 and 1985, respectively, and the Ph.D. degree in electrical engineering (optoelectronics) from the University of New Mexico, Albuquerque, in 1989.

From 1980 to 1986, he was a Research Engineer with the Agency for Defense Development. In 1986 to 1990, he was a Research Assistant, and later a Research Staff Member, at the Center for High Technology Materials, University of New Mexico. In 1990, he joined the faculty of Myong-Ji University, Korea, where he is currently a Professor with the Department of Electronics. From 1994 to 1995, he was a Visiting Research Fellow at the Photonics Research Laboratory, University of Melbourne, Melbourne, Australia. From 2002 to 2004, he was a Visiting Research Professor with the School of Electrical and Computer Engineering, Purdue University, West Lafayette, IN. His current research interests are in the areas of ultrashort optical pulse sources, very-high-speed optical data generation and transmission, semiconductor lasers, microwave photonics, and optical code-division multiple access (O-CDMA).

**D. E. Leaird** (M'01) was born in Muncie, IN, in 1964. He received the B.S. degree in physics from Ball State University, Muncie, IN, in 1987 and the M.S. and Ph.D. degrees from the School of Electrical and Computer Engineering, Purdue University, West Lafayette, IN, in 1996 and 2000, respectively.

In 1987, he joined Bell Communications Research (Bellcore), Red Bank, NJ, as a Senior Staff Technologist and later advanced to Member of Technical Staff. From 1987 to 1994, he worked in the Ultrafast Optics and Optical Signal Processing Research Group, where he was a key team member in research projects focusing on ultrafast optics, such as shaping of short optical pulses using liquid-crystal modulator arrays, investigation of dark soliton propagation in optical fibers, impulsive stimulated Raman scattering in molecular crystals, and all-optical switching. He is currently a Senior Research Scientist and Laboratory Manager of the Ultrafast Optics and Optical Fiber Communications Laboratory in the School of Electrical and Computer Engineering, Purdue University, where he has been since 1994. He has coauthored approximately 55 journal articles and 75 conference proceedings and has been issued one U.S. patent, with a second application pending.

Dr. Leaird is active in the optics community and professional organizations, including the Optical Society of America (OSA) and the IEEE Lasers & Electro-Optics Society (LEOS), where he is a member of the Ultrafast Technical Committee and serves as a consultant to venture capitalists by performing technical due diligence. He has received several awards for his work in the ultrafast optics field, including a Bellcore Award of Excellence, a Magoon Award for outstanding teaching, and an OSA/New Focus Student Award. He serves as a frequent reviewer for *Optics Letters*, *Applied Optics*, and the *Journal of the Optical Society of America B*, as well as for the IEEE PHOTONICS TECHNOLOGY LETTERS. In addition, he serves on the National Science Foundation review panels in the SBIR program.

**R. V. Roussev** received the M.Sc. degree in engineering physics (specializing in quantum electronics) from Sofia University, Bulgaria, in 1996. His M.Sc. thesis was in the field of nonlinear optics and photorefractive solitons. He is currently working toward the Ph.D. degree in applied physics at Stanford University, Stanford, CA.

From 1998 to 1999, he spent over a year as a Research Assistant in the Atomic Spectroscopy group at the Bulgarian Academy of Sciences, investigating transition probabilities and radiation lifetimes of excited states of Hg. His current research interests focus on developing efficient optical frequency conversion in periodically poled lithium niobate (bulk and waveguides) with increased resistance to photorefractive damage.

**C. Langrock** (S'01) received the physics diploma from the Heinrich–Heine–Universitdt, Düsseldorf, Germany, in 2001. He is currently working toward the Ph.D. degree in electrical engineering at Stanford University, Stanford, CA.

Currently, he is a Research Assistant in the Ginzton Laboratory at Stanford University. His research interests include single-photon generation and detection, detection of weak ultrashort optical pulses, and nonlinear optics.

**M. M. Fejer**, photograph and biography not available at the time of publication.

**A. M. Weiner** (S'84–M'84–SM'91–F'95) received the Sc.D. degree in electrical engineering from the Massachusetts Institute of Technology (MIT), Cambridge, in 1984.

From 1979 through 1984, he was a Fannie and John Hertz Foundation Graduate Fellow at MIT. In 1984, he joined Bellcore, at that time one of the premier research organizations in the telecommunications industry. In 1989, he was promoted to Manager of Ultrafast Optics and Optical Signal Processing. He joined Purdue University, West Lafayette, IN, in 1992 as Professor of Electrical and Computer Engineering, and is currently the Scifres Distinguished Professor of Electrical and Computer Engineering. From 1997 to 2003, he served as the ECE Director of Graduate Admissions. His research focuses on ultrafast optical signal processing and high-speed optical communications. He is especially well known for pioneering the field of femtosecond pulse shaping, which enables generation of nearly arbitrary ultrafast optical waveforms according to user specification. He has published four book chapters and more than 130 journal articles. He has been author or coauthor of more than 250 conference papers, including approximately 60 conference invited talks, and has presented over 70 additional invited seminars at universities or industry. He holds six U.S. patents.

Prof. Weiner is a Fellow of the Optical Society of America (OSA). He has received numerous awards for his research, including the Hertz Foundation Doctoral Thesis Prize (1984); the Adolph Lomb Medal of the Optical Society of America (1990), awarded for pioneering contributions to the field of optics made before age 30; the Curtis McGraw Research Award of the American Society of Engineering Education (1997); the International Commission on Optics Prize (1997); the IEEE Lasers & Electro-Optics Society (LEOS) William Streifer Scientific Achievement Award (1999); the Alexander von Humboldt Foundation Research Award for Senior U.S. Scientists (2000); and the inaugural Research Excellence Award from the Schools of Engineering at Purdue (2003). He has served on or chaired numerous research review panels, professional society award committees, and conference program committees. From 1988 to 1989, he served as an IEEE LEOS Distinguished Lecturer. He was General Co-Chair of the 1998 Conference on Lasers and Electro-optics, Chair of the 1999 Gordon Conference on Nonlinear Optics and Lasers, and Program Co-Chair of the 2002 International Conference on Ultrafast Phenomena. In addition, he has served as Associate Editor for the IEEE JOURNAL OF QUANTUM ELECTRONICS, IEEE PHOTONICS TECHNOLOGY LETTERS, and *Optics Letters*. He served as an elected member of the Board of Governors of IEEE LEOS from 1997 to 1999 and as Secretary/Treasurer of IEEE LEOS from 2000 to 2002. He is currently a Vice-President (representing IEEE LEOS) of the International Commission on Optics (ICO).